

Unveiling the Properties of Sulfhydryl Groups in a Single-Molecule Junction

Yanxia Xu, Jie Hao, Cong Zhao, Shaojia Li, Wei Si, Suhang He, Jinying Wang,* Chuancheng Jia,* and Xuefeng Guo*



Cite This: *Langmuir* 2024, 40, 7242–7248



Read Online

ACCESS |



Metrics & More

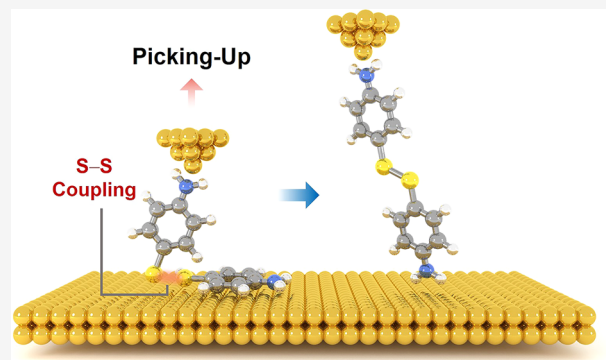


Article Recommendations



Supporting Information

ABSTRACT: The metal–thiol interface is ubiquitous in nanotechnology and surface chemistry. It is not only used to construct nanocomposites but also plays a decisive role in the properties of these materials. When organothiol molecules bind to the gold surface, there is still controversy over whether sulfhydryl groups can form disulfide bonds and whether these disulfide bonds can remain stable on the gold surface. Here, we investigate the intrinsic properties of sulfhydryl groups on the gold surface at the single-molecule level using a scanning tunneling microscope break junction technique. Our findings indicate that sulfhydryl groups can react with each other to form disulfide bonds on the gold surface, and the electric field can promote the sulfhydryl coupling reaction. In addition to these findings, ultraviolet irradiation is used to effectively regulate the coupling between sulfhydryl groups, leading to the formation and cleavage of disulfide bonds. These results unveil the intrinsic properties of sulfhydryl groups on the gold surface, therefore facilitating the accurate construction of broad nanocomposites with the desired functionalities.



INTRODUCTION

The self-assembly of organic sulfides or thiol derivatives on metal surfaces, due to their strong interaction with various metals such as gold and silver, is crucial for constructing nanocomposites,^{1–3} chemical sensors,^{4–7} and molecular-level electronic devices.^{8–12} It is generally believed that thiol groups adhere to the gold surface via gold–sulfur bonds, and this binding mechanism persists even in the presence of disulfide bonds, which can break to facilitate the formation of gold–sulfur bonds.^{13–15} Although the gold–sulfur interface has been studied using surface-enhanced Raman scattering spectroscopy, surface electrochemistry, and X-ray photoelectron spectroscopy,^{16–19} it is unclear whether sulfhydryl groups can interact with each other to form disulfide bonds and whether disulfide bonds can exist stably on the gold surface. Hence, it is necessary to conduct a comprehensive study on the state of sulfhydryl groups on the gold surface and their precise regulation at the single-molecule level.

Sulfhydryl groups are crucial for constructing single-molecule junctions as anchoring groups, making the single-molecule break junction technique an ideal method for characterizing the properties of sulfhydryl groups in organic sulfhydryl compounds. For instance, it has been demonstrated that the gold–sulfur interface coupling primarily occurs through chemical adsorption rather than physical adsorption during scanning tunneling microscope break junction (STM-

BJ) measurement in solution.²⁰ In addition, the disulfide-mediated dimerization process in benzene-1,4-dithiol has been investigated using mechanically controllable break junction and in situ surface-enhanced Raman spectroscopy.²¹ However, the universality of sulfhydryl coupling reactions and the stability of disulfide bonds on gold surfaces need to be further investigated. Moreover, applying external stimuli to the junction, such as light or electric fields, can easily trigger reactions, allowing control over the reactivity and selectivity of the interfacial reactions.²²

In this study, the STM-BJ technique is utilized to systematically investigate the binding states between the gold surface and sulfhydryl groups of a series of organic aromatic thiol compounds. The corresponding disulfide compound is used as a control, and the disulfide bond-breaking reagent is employed to disrupt disulfide bonds to ascertain whether disulfide bonds can form and remain stable on the gold surface. In addition, local electric fields and ultraviolet (UV) irradiation

Received: February 23, 2024

Revised: March 8, 2024

Accepted: March 8, 2024

Published: March 19, 2024



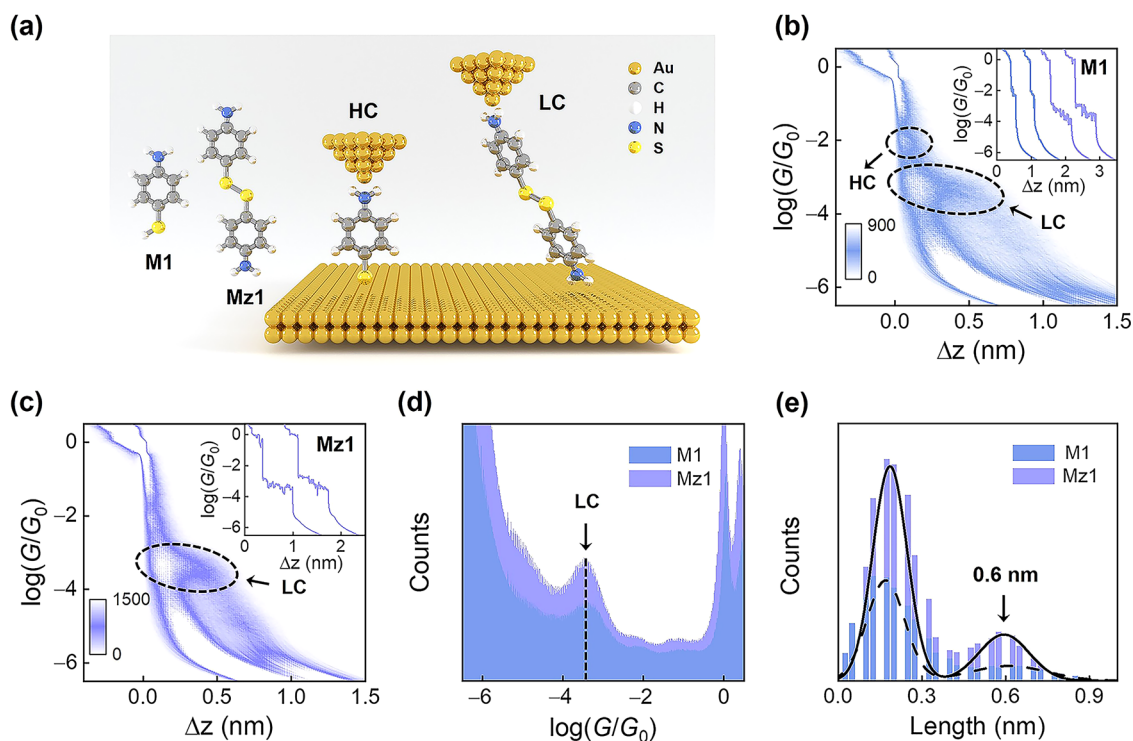


Figure 1. (a) Schematic of M1 and Mz1 single-molecule junctions. (b) 2D conductance–distance histogram of M1 measured at +100 mV. The individual conductance traces are shown in the insets. (c) 2D conductance–distance histogram of Mz1 measured at +100 mV. The insets show the conductance traces. (d) Corresponding 1D conductance histograms of M1 and Mz1. (e) Relative displacement distributions for the LC states of M1 and Mz1; peak centers are labeled by Gaussian fitting.

are introduced into the junctions to regulate the formation and breakage of disulfide bonds.

MATERIALS AND METHODS

Materials. 4-Aminothiophenol (M1, 97% purity), 4-mercaptopyridine (M2, 96% purity), 1,4-benzenedithiol (M3, 98% purity), biphenyl-4,4'-dithiol (M4, 98% purity), 4,4'-dithiodianiline (Mz1, 98% purity), 1,4-benzenediamine (98% purity), 4-(methylmercapto)aniline (98% purity), tris(2-carboxyethyl)phosphine hydrochloride (TCEP, 98% purity), and propylene carbonate (99% purity) were purchased from Macklin.

STM-BJ Measurements. Molecular junctions were created and analyzed using an Xtech STM-BJ from Xiamen University. Au substrates were obtained by vaporizing $\sim 10/200$ nm Cr/Au on a silicon wafer. During the STM-BJ experiment, 3 μ L of the 0.01 mM analyte solutions in propylene carbonate was directly dropped onto the surface of the Au substrate, which served as the foundation for subsequent experiments. The Au STM tips were made by electrochemical etching of 0.25 mm gold wires. To minimize background current, the used Au STM tips were coated with apiezon wax.²³ During single-molecule conductance measurements, the bias voltage between the Au substrate and the Au STM tip was 100 mV. The data analysis was conducted using the XMe open-source code.²⁴

***I*–*V* Characterizations.** The characterization of *I*–*V* curves was performed using the hovering mode.²⁵ When the conductance was within the preset conductance range ($10^{-4.0} G_0$ – $10^{-2.5} G_0$), the Au STM tip was halted and the bias voltage was scanned from -1 to 1 V, with a step of 0.5 mV. Finally, the individual *I*–*V* traces were collected to build a two-dimensional (2D) *I*–*V* histogram, and the fitting line was obtained by Gaussian fitting.²⁶

Flicker Noise Analysis. For the noise measurement, we employed the hovering mode of the STM-BJ equipment, maintaining the junction elongation for a duration of 200 ms after forming the molecular junction. Simultaneously, the conductance was collected at a certain bias voltage (100 mV) while applying a stretching rate (ν) of

9.3 nm/s. Only the traces with a sufficient junction duration were eligible for extraction and subsequent analysis through discrete Fourier transformation. During this transformation, these traces were squared to derive the noise power spectra density (PSD). The study range of flicker noise typically falls within the frequency band of 100–1000 Hz, primarily due to constraints related to the mechanical stability of the experimental setup and the presence of background noise. Then, the PSD was integrated over the frequency range of 100–1000 Hz to obtain the normalized flicker noise power (noise power/ G_{AVG}). Finally, the 2D histograms of noise power/ G_{AVG} and noise power/ G_{AVG}^n versus G_{AVG} were plotted to directly reflect the correlation between the two variables, where n is called the scaling exponent of the G_{AVG} .^{27–29} In a through-space coupled system, the flicker noise power scales with G_{AVG}^2 . The noise power distribution is a slanted ellipse, and the scaling exponent n is 2. In a through-bond coupled system, the flicker noise power scales with G_{AVG} . The noise in 2D histograms of noise power/ G_{AVG} presents an orthogonal elliptic distribution, and the scaling exponent n is 1.

Theoretical Calculations. The transmission spectra of M1 and Mz1 molecular junctions were calculated after geometry optimization employing density functional theory (DFT) within the non-equilibrium Green's function (NEGF) formalism.^{30,31} The calculations were performed using the Atomistix Toolkit (ATK) package. FHI pseudopotentials (double- ζ polarized) were employed in the NEGF-DFT calculation at the PBE level, with a cutoff energy of 150 Ha and a k -point grid of $4 \times 4 \times 150$. For the transmission spectrum calculation, the k -point sampling was set to 7.

RESULTS AND DISCUSSION

Exploring Single-Molecule Sulfhydryl Coupling Reactions on the Gold Surface. Specifically, the 4-aminothiophenol (M1) molecule (Figure 1a) is first used to characterize the possible states of sulfhydryl groups. Experimental details of STM-BJ measurements are described in the Materials and Methods section. Over 10,000 individual

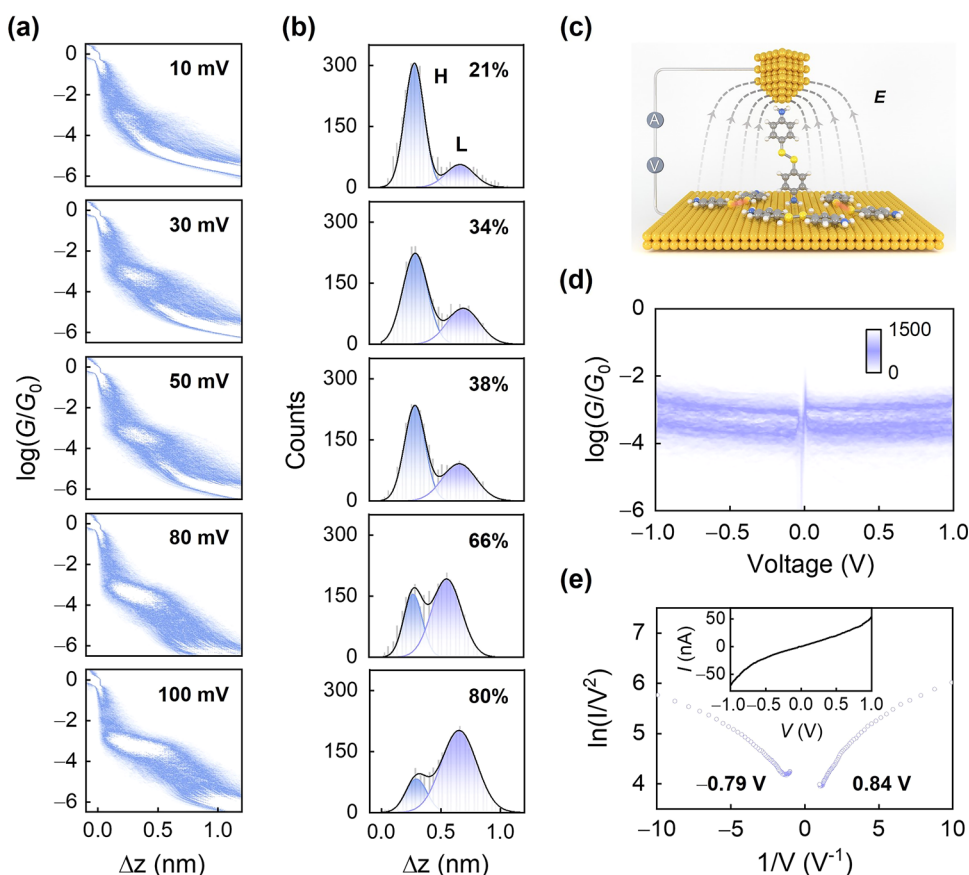


Figure 2. (a) 2D conductance–distance histograms of M1 measured under different bias voltages, where the tunneling traces are screened out. (b) Corresponding relative displacement distributions, where the peaks are fitted by the Gaussian function. Peaks labeled as H and L come from the traces containing HC and LC states, respectively. (c) Schematic illustrating the coupling of two M1 molecules driven by the local electric field in the molecular junction. (d) 2D conductance versus voltage (G – V) histogram of the LC state for M1. (e) Transition voltage spectra (TVS) constructed from the fitted I – V curve (black line) in Figure S4. The inset shows the corresponding I – V curve.

conductance–distance traces are collected to construct the 2D conductance–distance histogram for M1 (Figure 1b). This histogram reveals two conductance plateaus circled by dashed lines at $\sim 10^{-2.0} G_0$ (≈ 775.0 nS) and $\sim 10^{-3.5} G_0$ (≈ 24.5 nS), which correspond to high-conductance (HC) and low-conductance (LC) states, respectively, where G_0 represents quantum conductance ($2e^2/h$, $77.5 \mu\text{S}$).³² Two types of individual conductance traces involving HC and LC states are shown in the inset of Figure 1b. Notably, the molecular plateau of the LC state (~ 0.60 nm) exceeds that of the HC state (~ 0.15 nm). The HC state aligns with some previous reports of the M1 single-molecule junction (Figure 1a).³³

There are two most probable hypotheses for the origin of the LC state: one is the formation of 4,4'-dithiodianiline (Mz1) via sulfhydryl coupling reactions and the other is the formation of 4,4'-dimercaptoazobenzene through amino coupling reactions. To prove whether the former is reasonable, single-molecule conductance experiments on Mz1 are carried out. The 2D conductance–distance and 1D conductance histograms show that Mz1 exhibits almost identical conductance characteristics to M1 (Figure 1c,d). The conductance values of LC states in both M1 and Mz1 are almost identical, which are around $\sim 10^{-3.5} G_0$ (≈ 24.5 nS). To further confirm that HC and LC states come from M1 and Mz1 single-molecule junctions (Figure 1a), respectively, DFT in combination with the NEFG method is employed to simulate the transport behavior of M1 and Mz1 single-molecule

junctions at zero bias voltage. The transmission spectrum (Figure S1) reveals that the conductance of M1 is approximately 2 orders of magnitude larger than that of Mz1, which is in accordance with the experimental conductance difference. In addition, the most probable relative displacements of the LC states in M1 and Mz1 are also analyzed, and the results show that the corresponding plateau lengths for the LC states in both M1 and Mz1 are ~ 0.6 nm (Figure 1e). Notably, a high-conductance feature similar to that of M1, ranging from $\sim 10^{-2.3} G_0$ (≈ 338.4 nS) to $\sim 10^{-1.8} G_0$ (≈ 1228.3 nS), is observed in Figure 1c,d. This suggests that Mz1 may also form a stable junction in another configuration with an amino group and a sulfur atom anchored to the two gold electrodes, respectively.

To further verify the existence of the S–S bond, propylene carbonate-dissolved saturated tris(2-carboxyethyl)phosphine hydrochloride (TCEP) solution, capable of triggering the cleavage of disulfide bonds, is added into the M1 and Mz1 solutions during the single-molecule conductance measurements.³⁴ As shown in Figure S2, the LC states of M1 and Mz1 almost disappear after the addition of TCEP, while the HC states remain unchanged. Furthermore, a series of aniline derivatives that are not modified by sulfhydryl groups are also studied to rule out the occurrence of amino coupling reactions. Figure S3 illustrates that no new conductance peaks can be found in 2D conductance–distance histograms except for those of the molecules themselves, indicating that the coupling

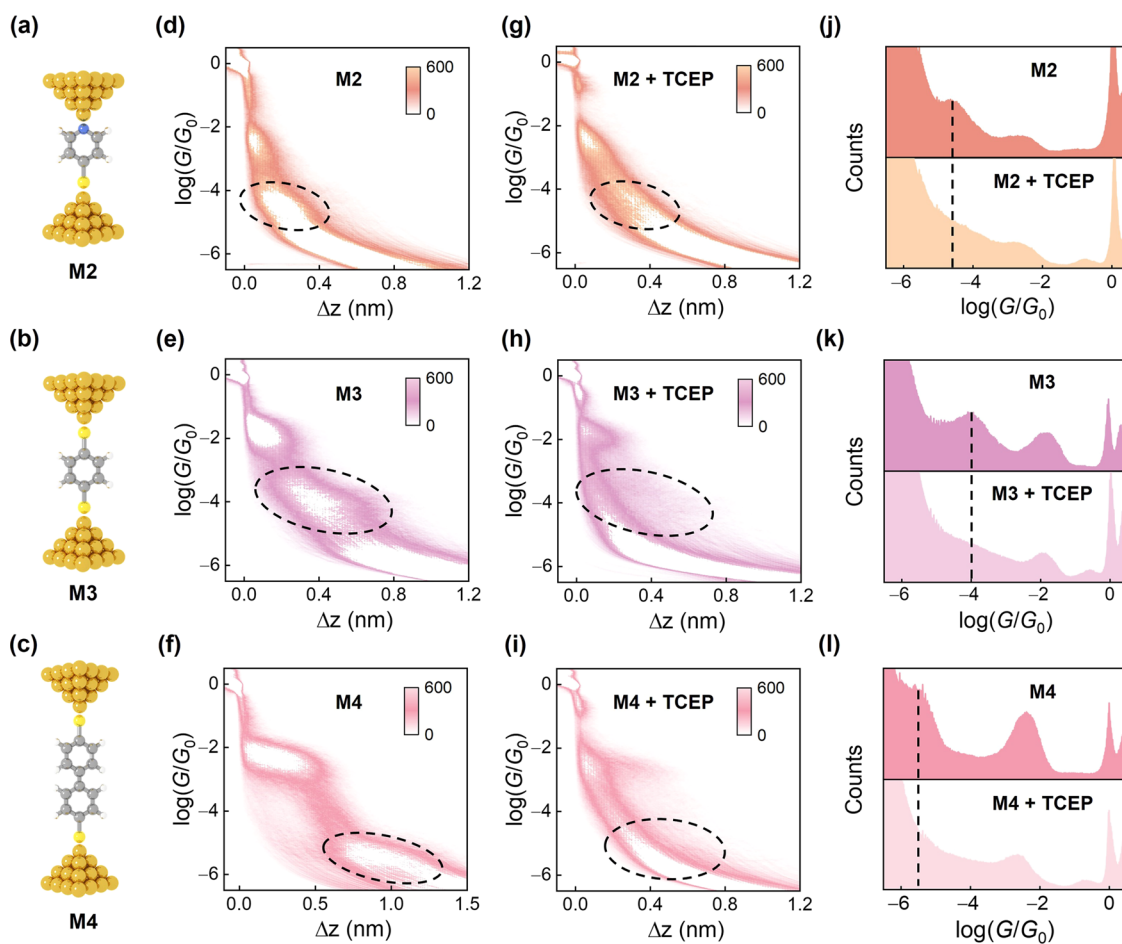


Figure 3. (a–c) Schematic of the M2–M4 single-molecule junctions, where M2–M4 represents 4-mercaptopyridine, 1,4-benzenedithiol, and biphenyl-4,4'-dithiol, respectively. (d–f) 2D conductance–distance histograms of M2–M4. (g–i) 2D conductance–distance histograms of M2–M4 after the addition of TCEP. (j–l) 1D conductance histograms of M2–M4 before (up) and after (down) the addition of TCEP.

reaction between amino groups on the Au substrate does not occur at the test bias voltage. Note that previous studies³³ have shown that the conductance of 4,4'-dimercaptoazobenzene fell within the range from $\sim 10^{-2.8} G_0$ (≈ 122.8 nS) to $\sim 10^{-1.8} G_0$ (≈ 1228.3 nS), exceeding the conductance value of the LC state in M1. Moreover, the Au-catalyzed amino oxidative coupling reactions can only be driven when the electrochemical potential of the Au STM tip is sufficiently high. All of this evidence confirms that the newly formed LC state in M1 comes from the Mz1 single-molecule junction, which is the result of the sulfhydryl coupling reaction of M1.

Electric Field Regulated Sulfhydryl Coupling Reactions on the Gold Surface. It is widely recognized that an oriented external electric field can be generated within the nanogap between the two STM electrodes. The application of a strong external electric field can alter the potential of the gold surface, thereby regulating the interfacial sulfhydryl coupling reaction.²² To substantiate this assumption, bias-dependent measurements of M1 are carried out. In the measurements, the bias voltage changes from 10 to 100 mV. Figure 2a illustrates the 2D conductance–distance histograms under different bias voltages. At low bias voltages, the proportion of the LC state originating from the sulfhydryl coupled product is small; with the increase of the bias voltage, the LC state becomes more pronounced. To quantitatively analyze the formation probability of sulfhydryl coupled product, the displacement

distribution is further extracted (Figure 2b). Two peaks appear in the displacement distribution, where the peaks labeled with L and H come from traces containing HC and LC states, respectively. Thus, the probability of sulfhydryl coupling can be determined by the proportion of the peak L. When the bias voltage increases from 10 to 100 mV, the junction formation probability (JFP) of the LC state increases from 21 to 80% (Figure 2b), indicating that the local electric field can promote the sulfhydryl coupling reaction. Corresponding control experiments of Mz1 are performed to eliminate other influencing factors (Figure S4). The JFP of the LC state for Mz1 remains almost constant as the bias voltage increases. It is evident that the enhancement of the local electric field promotes the sulfhydryl coupling reaction, consequently increasing the JFP of the LC state for M1 (Figure 2c).

To prove that S–S bonds can stably exist on the gold surface under high bias voltage, the I – V and G – V characteristics based on the LC state of M1 are investigated (Figures S4 and 2d). According to the 2D G – V histogram, it is evident that the conductance of the LC state remains constant regardless of the bias voltage, indicating that the S–S bond remains highly stable even under high bias voltage conditions, displaying excellent conductivity. To obtain a deeper understanding of charge transfer characteristics, the transition voltage spectrum (TVS), which is the Fowler–Nordheim plot ($\ln(I/V^2)$ versus $1/V$), is analyzed (Figure 2e). The transition voltage (V_{trans}) is

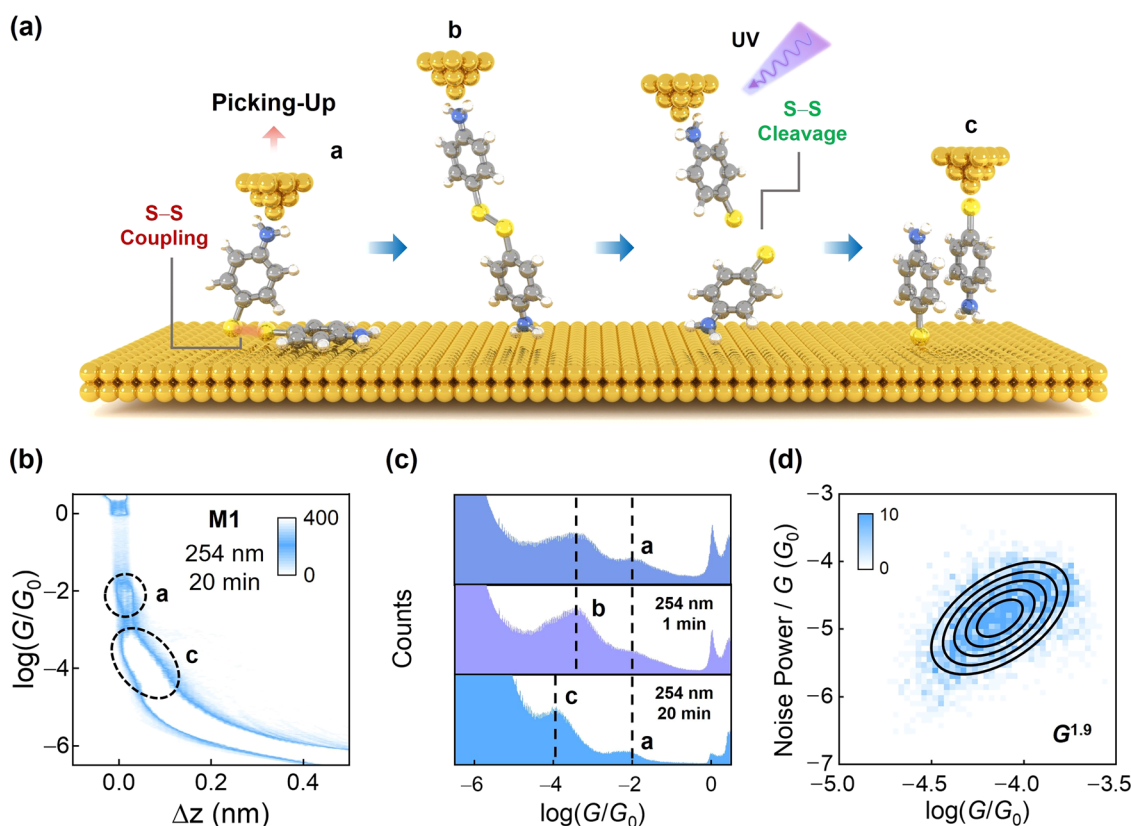


Figure 4. (a) Schematic of the M1 molecular junction measured under UV irradiation. (b) 2D conductance–distance histogram of M1 after 20 min of UV irradiation. (c) 1D conductance histograms of M1 at different UV irradiation times. (d) 2D histogram of flicker noise power versus average conductance for M1 junctions corresponding to the LC state in (b).

identified as the minimum point in the TVS.^{35–37} It can be observed that the absolute V_{trans} value of the LC state in M1 is about 0.8 V, indicating that the G – V data in Figure 2d originate from the Mz1 molecular junctions.

Universality of Sulfhydryl Coupling Reactions. To explore the generality of the sulfhydryl coupling reaction, other thiophenol derivatives (M2–M4) with different backbones and terminal groups are studied (Figure 3a–3c). The 2D conductance–distance histograms for M2–M4 show two conductance features (Figure 3d–3f). Similarly, the formation of S–S bonds is further verified by the addition of the disulfide bond-breaking reagent TCEP during the single-molecule conductance measurements. As shown in Figure 3g–3l, the LC states of M2–M4 almost disappear after the addition of TCEP, while the HC states still exist, indicating that the presence of low-conductance peaks circled by dashed lines represents the formation of Mz2–Mz4 (molecular structures shown in Figure S5) via the sulfhydryl coupling reaction.

Effect of UV Irradiation on Sulfhydryl Reactions. Disulfide bonds can be formed or broken under specific conditions, including heating, pH, and light.³⁸ Among these conditions, light is an effective means of triggering and controlling chemical reactions. Studies have demonstrated that molecules containing disulfide bonds (~ 240 kJ/mol) can exchange with each other when exposed to UV irradiation, a process known as photodissociation.³⁸ To achieve precise control of these photochemical reactions, a UV light source at ~ 254 nm is employed for irradiating the analyte solution containing M1 during the STM-BJ measurement (Figure 4a). Before UV irradiation, the 2D conductance–distance histo-

gram displays two distinct conductance plateaus, denoted as 'a' and 'b' in Figure S6a. Here, 'a' corresponds to the conductance state of the M1 junction, while 'b' represents the conductance state of the Mz1 junction, arising from the sulfhydryl coupling reaction between M1, as described above. After 1 min of irradiation, compared to the nonirradiated condition, the intensity of the 'b' conductance peak increases (Figure S6b). This is because UV light can induce photochemical reactions of M1 to produce sulfenyl radicals, which have high reactivity to form disulfide bonds. With an extended illumination time of 20 min, a new low-conductance peak labeled 'c' emerges, registering a conductance value of $\sim 10^{-4.1} G_0$ (≈ 6.2 nS). However, the high-conductance peak 'a' remains constant (Figure 4b,4c). This observation suggests that UV light can further break the previously formed disulfide bonds, leading to gold–sulfur binding, akin to what occurs with 'a' in Figure 4a. Concurrently, π – π stacking between M1 molecules may occur during the break junction process, represented by 'c' in Figure 4a. To further verify that the low-conductance peak 'c' originates from stacked molecular junctions formed through the intermolecular π – π stacking effect involving M1, flicker noise analysis on the low-conductance peak 'c' is performed. As shown in Figure 4d, it can be observed that the noise power scale for 'c' is $G^{1.9}$, indicating that the π – π stacked molecular junction is the main charge transport pathway.^{27–29}

CONCLUSIONS

In summary, the properties of sulfhydryl groups on the gold surface have been explored at the single-molecule level. Extensive experiments have proven that sulfhydryl groups in

various molecules can indeed react with each other to form stable disulfide bonds on the gold surface. It is found that the electric field applied to the molecules can accelerate the coupling reaction between sulfhydryl groups. In addition, UV irradiation has been shown to effectively modulate the formation and cleavage of disulfide bonds. These findings establish a foundation for precise control over the reaction and self-assembly of organic aromatic sulfhydryl molecules, facilitating a wide range of applications, including nano-electronic device fabrication, surface modification, nanomaterial synthesis, and molecular recognition and detection.

■ ASSOCIATED CONTENT

SI Supporting Information

The Supporting Information is available free of charge at <https://pubs.acs.org/doi/10.1021/acs.langmuir.4c00644>.

Transmission spectra of M1 and Mz1; STM-BJ measurements of M1 and Mz1 before and after the addition of TCEP; STM-BJ measurements of 1,4-benzenediamine and 4-(methylmercapto)aniline; STM-BJ measurements of Mz1 under different bias voltages; molecular structures of Mz2–Mz4; and STM-BJ measurements of M1 under different UV irradiation time (PDF)

■ AUTHOR INFORMATION

Corresponding Authors

Jinying Wang – Network for Computational Nanotechnology, School of Electrical and Computer Engineering, Purdue University, West Lafayette, Indiana 47907, United States; Email: wang4205@purdue.edu

Chuan Cheng Jia – Center of Single-Molecule Sciences, Institute of Modern Optics, Frontiers Science Center for New Organic Matter, Tianjin Key Laboratory of Micro-scale Optical Information Science and Technology, College of Electronic Information and Optical Engineering, Nankai University, Tianjin 300350, P. R. China; Email: jiacc@nankai.edu.cn

Xuefeng Guo – Center of Single-Molecule Sciences, Institute of Modern Optics, Frontiers Science Center for New Organic Matter, Tianjin Key Laboratory of Micro-scale Optical Information Science and Technology, College of Electronic Information and Optical Engineering, Nankai University, Tianjin 300350, P. R. China; Beijing National Laboratory for Molecular Sciences, National Biomedical Imaging Center, College of Chemistry and Molecular Engineering, Peking University, Beijing 100871, P. R. China; orcid.org/0000-0001-5723-8528; Email: guoxf@pku.edu.cn

Authors

Yanxia Xu – Center of Single-Molecule Sciences, Institute of Modern Optics, Frontiers Science Center for New Organic Matter, Tianjin Key Laboratory of Micro-scale Optical Information Science and Technology, College of Electronic Information and Optical Engineering, Nankai University, Tianjin 300350, P. R. China; orcid.org/0000-0001-5339-4638

Jie Hao – Center of Single-Molecule Sciences, Institute of Modern Optics, Frontiers Science Center for New Organic Matter, Tianjin Key Laboratory of Micro-scale Optical Information Science and Technology, College of Electronic Information and Optical Engineering, Nankai University, Tianjin 300350, P. R. China

Cong Zhao – Center of Single-Molecule Sciences, Institute of Modern Optics, Frontiers Science Center for New Organic Matter, Tianjin Key Laboratory of Micro-scale Optical Information Science and Technology, College of Electronic Information and Optical Engineering, Nankai University, Tianjin 300350, P. R. China

Shaojia Li – Center of Single-Molecule Sciences, Institute of Modern Optics, Frontiers Science Center for New Organic Matter, Tianjin Key Laboratory of Micro-scale Optical Information Science and Technology, College of Electronic Information and Optical Engineering, Nankai University, Tianjin 300350, P. R. China

Wei Si – Center of Single-Molecule Sciences, Institute of Modern Optics, Frontiers Science Center for New Organic Matter, Tianjin Key Laboratory of Micro-scale Optical Information Science and Technology, College of Electronic Information and Optical Engineering, Nankai University, Tianjin 300350, P. R. China

Suhang He – Center of Single-Molecule Sciences, Institute of Modern Optics, Frontiers Science Center for New Organic Matter, Tianjin Key Laboratory of Micro-scale Optical Information Science and Technology, College of Electronic Information and Optical Engineering, Nankai University, Tianjin 300350, P. R. China

Complete contact information is available at:

<https://pubs.acs.org/10.1021/acs.langmuir.4c00644>

Author Contributions

X.G., C.J., and J.W. conceived the idea for the paper. Y.X. carried out the experimental measurements. J.H. performed the theoretical calculations. X.G., C.J., J.W., Y.X., C.Z., S.L., W.S., and S.H. analyzed the data and wrote the paper.

Notes

The authors declare no competing financial interest.

■ ACKNOWLEDGMENTS

The authors acknowledge primary financial supports from the Natural Science Foundation of Beijing (2222009), the National Key R&D Program of China (2022YFE0128700, 2021YFA1200102, and 2021YFA1200101), the National Natural Science Foundation of China (22173050, 21727806, 22150013, and 21933001), Beijing National Laboratory for Molecular Sciences (BNLMS202105), “Frontiers Science Center for New Organic Matter” at Nankai University (63181206), the New Cornerstone Science Foundation through the XPLOER PRIZE, and the Fundamental Research Funds for the Central Universities (63223056).

■ REFERENCES

- (1) Love, J. C.; Estroff, L. A.; Kriebel, J. K.; Nuzzo, R. G.; Whitesides, G. M. Self-Assembled Monolayers of Thiolates on Metals as a Form of Nanotechnology. *Chem. Rev.* **2005**, *105* (4), 1103–1170.
- (2) Häkkinen, H. The Gold-Sulfur Interface at the Nanoscale. *Nat. Chem.* **2012**, *4* (6), 443–455.
- (3) Vericat, C.; Vela, M. E.; Benitez, G.; Carro, P.; Salvarezza, R. C. Self-Assembled Monolayers of Thiols and Dithiols on Gold: New Challenges for a Well-Known System. *Chem. Soc. Rev.* **2010**, *39* (5), 1805–1834.
- (4) Singh, M.; Kaur, N.; Comini, E. The Role of Self-Assembled Monolayers in Electronic Devices. *J. Mater. Chem. C* **2020**, *8* (12), 3938–3955.

- (5) Minami, T. Organic Transistor-Based Chemical Sensors with Self-Assembled Monolayers. *J. Incl. Phenom. Macrocycl. Chem.* **2021**, *101* (1), 1–18.
- (6) Flink, S.; van Veggel, F. C.; Reinhoudt, D. N. Sensor Functionalities in Self-Assembled Monolayers. *Adv. Mater.* **2000**, *12* (18), 1315–1328.
- (7) Arya, S. K.; Solanki, P. R.; Datta, M.; Malhotra, B. D. Recent Advances in Self-Assembled Monolayers Based Biomolecular Electronic Devices. *Biosens. Bioelectron.* **2009**, *24* (9), 2810–2817.
- (8) Nijhuis, C. A.; Reus, W. F.; Whitesides, G. M. Molecular Rectification in Metal-SAM-Metal-Oxide-Metal Junctions. *J. Am. Chem. Soc.* **2009**, *131* (49), 17814–17827.
- (9) Wang, W.; Lee, T.; Reed, M. A. Mechanism of Electron Conduction in Self-Assembled Alkanethiol Monolayer Devices. *Phys. Rev. B* **2003**, *68* (3), No. 035416.
- (10) Fan, F. R. F.; Yang, J.; Cai, L.; Price Jr, D. W.; Dirk, S. M.; Kosynkin, D. V.; Yao, Y.; Rawlett, A. M.; Tour, J. M.; Bard, A. J. Charge Transport through Self-Assembled Monolayers of Compounds of Interest in Molecular Electronics. *J. Am. Chem. Soc.* **2002**, *124* (19), 5550–5560.
- (11) Liu, Y.; Qiu, X.; Soni, S.; Chiechi, R. C. Charge Transport through Molecular Ensembles: Recent Progress in Molecular Electronics. *Chem. Phys. Rev.* **2021**, *2* (2), No. 021303.
- (12) Li, P.; Chen, Y.; Wang, B.; Li, M.; Xiang, D.; Jia, C.; Guo, X. Single-Molecule Optoelectronic Devices: Physical Mechanism and Beyond. *Opto-Electron. Adv.* **2022**, *5* (5), No. 210094.
- (13) Nuzzo, R. G.; Aliara, D. L. Adsorption of Bifunctional Organic Disulfides on Gold Surfaces. *J. Am. Chem. Soc.* **1983**, *105* (13), 4483–4484.
- (14) Grönbeck, H.; Curioni, A.; Andreoni, W. Thiols and Disulfides on the Au(111) Surface: The Headgroup-Gold Interaction. *J. Am. Chem. Soc.* **2000**, *122* (16), 3839–3842.
- (15) Takata, L. M. S.; Gonçalves, A. C.; Ando, R. A.; Dos Santos, A. A.; Camargo, P. H. Functionalization of Gold and Silver Nanoparticles with Diphenyl Dichalcogenides Probed by Surface Enhanced Raman Scattering. *J. Raman Spectrosc.* **2012**, *43* (6), 712–717.
- (16) Szafranski, C. A.; Tanner, W.; Laibinis, P. E.; Garrell, R. L. Surface-Enhanced Raman Spectroscopy of Aromatic Thiols and Disulfides on Gold Electrodes. *Langmuir* **1998**, *14* (13), 3570–3579.
- (17) Madzharova, F.; Heiner, Z.; Kneipp, J. Surface-Enhanced Hyper Raman Spectra of Aromatic Thiols on Gold and Silver Nanoparticles. *J. Phys. Chem. C* **2020**, *124* (11), 6233–6241.
- (18) Walczak, M. M.; Alves, C. A.; Lamp, B. D.; Porter, M. D. Electrochemical and X-ray Photoelectron Spectroscopic Evidence for Differences in the Binding Sites of Alkanethiolate Monolayers Chemisorbed at Gold. *J. Electroanal. Chem.* **1995**, *396* (1–2), 103–114.
- (19) Cossaro, A.; Mazzarello, R.; Rousseau, R.; Casalis, L.; Verdini, A.; Kohlmeyer, A.; Floreano, L.; Scandolo, S.; Morgante, A.; Klein, M. L.; Scoles, G. X-ray Diffraction and Computation Yield the Structure of Alkanethiols on Gold(111). *Science* **2008**, *321* (5891), 943–946.
- (20) Inkpen, M. S.; Liu, Z.; Li, H.; Campos, L. M.; Neaton, J. B.; Venkataraman, L. Non-Chemisorbed Gold-Sulfur Binding Prevails in Self-Assembled Monolayers. *Nat. Chem.* **2019**, *11* (4), 351–358.
- (21) Zheng, J.; Liu, J.; Zhuo, Y.; Li, R.; Jin, X.; Yang, Y.; Chen, Z.; Shi, J.; Xiao, Z.; Hong, W.; Tian, Z. Q. Electrical and SERS Detection of Disulfide-Mediated Dimerization in Single-Molecule Benzene-1,4-Dithiol Junctions. *Chem. Sci.* **2018**, *9* (22), 5033–5038.
- (22) Chen, H.; Jia, C.; Zhu, X.; Yang, C.; Guo, X.; Stoddart, J. F. Reactions in Single-Molecule Junctions. *Nat. Rev. Mater.* **2023**, *8* (3), 165–185.
- (23) Nagahara, L. A.; Thundat, T.; Lindsay, S. M. Preparation and Characterization of STM Tips for Electrochemical Studies. *Rev. Sci. Instrum.* **1989**, *60* (10), 3128–3130.
- (24) Pan, Z.; Dong, G.; Shang, C.; Li, R.; Gao, T.; Lin, L.; Duan, H.; Li, X.; Bai, J.; Lai, Y.; et al. Xme - Xiamen Molecular Electronics code: An Intelligent and Open-Source Data Analysis Tool for Single-Molecule Conductance Measurements. *Chin. J. Chem.* **2024**, *42* (3), 317–329.
- (25) Lovat, G.; Choi, B.; Paley, D. W.; Steigerwald, M. L.; Venkataraman, L.; Roy, X. Room-Temperature Current Blockade in Atomically Defined Single-Cluster Junctions. *Nat. Nanotechnol.* **2017**, *12* (11), 1050–1054.
- (26) Huisman, E. H.; Guédon, C. M.; van Wees, B. J.; van der Molen, S. J. Interpretation of Transition Voltage Spectroscopy. *Nano Lett.* **2009**, *9* (11), 3909–3913.
- (27) Adak, O.; Rosenthal, E.; Meisner, J.; Andrade, E. F.; Pasupathy, A. N.; Nuckolls, C.; Hybertsen, M. S.; Venkataraman, L. Flicker Noise as a Probe of Electronic Interaction at Metal-Single Molecule Interfaces. *Nano Lett.* **2015**, *15* (6), 4143–4149.
- (28) Yuan, S.; Gao, T.; Cao, W.; Pan, Z.; Liu, J.; Shi, J.; Hong, W. The Characterization of Electronic Noise in the Charge Transport through Single-Molecule Junctions. *Small Methods* **2021**, *5* (3), No. 2001064.
- (29) Pan, Z.; Chen, L.; Tang, C.; Hu, Y.; Yuan, S.; Gao, T.; Shi, J.; Shi, J.; Yang, Y.; Hong, W. The Evolution of the Charge Transport Mechanism in Single-Molecule Break Junctions Revealed by Flicker Noise Analysis. *Small* **2022**, *18* (10), No. 2107220.
- (30) Taylor, J.; Guo, H.; Wang, J. Ab Initio Modeling of Quantum Transport Properties of Molecular Electronic Devices. *Phys. Rev. B* **2001**, *63* (24), No. 245407.
- (31) Brandbyge, M.; Mozos, J.; Ordejón, P.; Taylor, J.; Stokbro, K. Density-Functional Method for Nonequilibrium Electron Transport. *Phys. Rev. B* **2002**, *65* (16), No. 165401.
- (32) Yanson, A. I.; Bollinger, G. R.; van den Brom, H. E.; Agrait, N.; van Ruitenbeek, J. M. Formation and Manipulation of a Metallic Wire of Single Gold Atoms. *Nature* **1998**, *395* (6704), 783–785.
- (33) Zang, Y.; Stone, I.; Inkpen, M. S.; Ng, F.; Lambert, T. H.; Nuckolls, C.; Steigerwald, M. L.; Roy, X.; Venkataraman, L. In Situ Coupling of Single Molecules Driven by Au-Catalyzed Electro-oxidation. *Angew. Chem. Int. Ed.* **2019**, *58* (45), 16008–16012.
- (34) Burns, J. A.; Butler, J. C.; Moran, J.; Whitesides, G. M. Selective Reduction of Disulfides by Tris(2-carboxyethyl)phosphine. *J. Org. Chem.* **1991**, *56* (8), 2648–2650.
- (35) Song, H.; Kim, Y.; Jang, Y.; Jeong, H.; Reed, M. A.; Lee, T. Observation of Molecular Orbital Gating. *Nature* **2009**, *462* (7276), 1039–1043.
- (36) Guo, S.; Hihath, J.; Díez-Pérez, I.; Tao, N. Measurement and Statistical Analysis of Single-Molecule Current Voltage Characteristics, Transition Voltage Spectroscopy, and Tunneling Barrier Height. *J. Am. Chem. Soc.* **2011**, *133* (47), 19189–19197.
- (37) Beebe, J. M.; Kim, B.; Gadzuk, J. W.; Frisbie, C. D.; Kushmerick, J. G. Transition from Direct Tunneling to Field Emission in Metal-Molecule-Metal Junctions. *Phys. Rev. Lett.* **2006**, *97* (2), No. 026801.
- (38) Fan, F.; Ji, S.; Sun, C.; Liu, C.; Yu, Y.; Fu, Y.; Xu, H. Wavelength-Controlled Dynamic Metathesis: A Light-Driven Exchange Reaction Between Disulfide and Diselenide Bonds. *Angew. Chem. Int. Ed.* **2018**, *57* (50), 16426–16430.